

Article

Simulation and Validation of Thickness of Slag Crust on the Copper Stave in the High-Temperature Area of Blast Furnace

Dongliang Liu ^{1,2}, Wei Zhang ^{1,*} , Zhengliang Xue ^{1,*}, Chunhui Song ³ and Lingkun Chen ²

¹ The State Key Laboratory of Refractories and Metallurgy, Wuhan University of Science and Technology, Wuhan 430081, China

² Baosteel Central Research Institute (R&D Center of Wuhan Iron & Steel Co., Ltd.), Wuhan 430080, China

³ Wuhan Branch of Xiangyang Heavy Equipment Materials Co., Ltd., Wuhan 430080, China

* Correspondence: wei_zhang@wust.edu.cn (W.Z.); xuezhengliang@wust.edu.cn (Z.X.)

Abstract: The blast furnace is the dominant high-temperature reactor in the modern ironmaking industry. Iron oxide in iron ores can be converted to metallic iron through blast furnace smelting, and this high-temperature melting can be used to separate the molten iron from the gangue components. The formation and thickness of the hot-surface slag crust on the copper stave in the high-temperature area of the middle and lower parts of the blast furnace are crucial for the safe operation and long campaign of the blast furnace. To enhance the precision of determining the thickness of the slag crust in this specific region, samples were extracted from the hot surface of the copper cooler situated in the high-temperature area. This extraction was carried out during the maintenance procedure of the blast furnace stockline. Subsequently, the thermal conductivity and melting performance of the slag crust were measured. The slag crust thicknesses corresponding to the various temperature measurement sites of the stave were determined by developing a mathematical model for the heat transfer of the copper stave. The actual slag crust thickness measurement data were acquired while the blast furnace stockline was in operation, and the data were then utilized to corroborate the model's predictions. A blast furnace with an effective volume of 3200 m³ was used to test the model. The average thickness of the hot-surface slag crust was computed for cases that occurred between 2020 and 2022. The data's correlations with the blast furnace's technical and economic indices during the same time period were examined. The findings indicated that the blast furnace's operation indices improved with a thinner slag crust, but there was also a higher chance of damage to the copper stave's internal cooling water pipes. Taking into account the technical and economic indices as well as a long campaign of the blast furnace, 150–200 mm is recommended as the appropriate average slag crust thickness on the surface of the copper stave in the high-temperature section.



Citation: Liu, D.; Zhang, W.; Xue, Z.; Song, C.; Chen, L. Simulation and Validation of Thickness of Slag Crust on the Copper Stave in the High-Temperature Area of Blast Furnace. *Metals* **2024**, *14*, 19. <https://doi.org/10.3390/met14010019>

Academic Editors: Mark E. Schlesinger and Petros E. Tsakiridis

Received: 17 November 2023

Revised: 13 December 2023

Accepted: 20 December 2023

Published: 22 December 2023



Copyright: © 2023 by the authors. Licensee MDPI, Basel, Switzerland. This article is an open access article distributed under the terms and conditions of the Creative Commons Attribution (CC BY) license (<https://creativecommons.org/licenses/by/4.0/>).

1. Introduction

The blast furnace is usually recognized as a perfect high-temperature reactor in the modern ironmaking industry [1–3]. Iron ore and coke enter the high-temperature reactor from the upper throat of the blast furnace, while high-temperature and high-pressure blast and auxiliary fuel enter the reactor from the lower tuyere of the blast furnace [4–7]. The high-temperature gas generated by the combustion of fuel in the tuyere area of the blast furnace rises in a countercurrent with the downward moving burden. The CO in the gas reduces the iron oxide in the iron ore into metallic iron while transferring heat to the burden. Through a series of complex physical and chemical interactions, the melting and separation of slag and iron are achieved [8–10]. The blast furnace is a large and efficient reactor that operates continuously, and the long campaign of modern large blast furnaces can reach 15–20 years. Within 0.5 to 3 years after the blast furnace is opened, the bricks on the hot surface of the stave above the tuyeres are almost completely detached. The stave

mainly relies on the slag crust on the hot surface to protect it and form a working furnace shape. The high-temperature area of a blast furnace refers to the bosh, waist, and lower shaft of the furnace body above the tuyere. The working state of the stave in this area is crucial for the smooth operation and long campaign of the blast furnace [11]. The thermal conductivity of a copper stave is much higher than that of a foundry iron stave, and the high thermal conductivity of a copper stave makes it easier to quickly form slag crust protection. Therefore, since the beginning of this century, copper staves have been chosen in the bosh, waist, and lower shaft of the furnace body in many newly built and overhauled blast furnaces. However, due to the fact that the blast furnace is a high-temperature and high-pressure reactor, it is difficult to directly monitor the thickness of the hot-surface slag crust of the copper stave, and the appropriate slag crust thickness is difficult to determine and control, resulting in frequent thickening of the furnace wall and damage to the stave in the operation of the blast furnace. For example, a 3200 m³ blast furnace, which was put into operation in 2006, had frequent thickening on the copper stave in 2015. From 2020 to 2022, there were many cases of copper stave damage, and it was forced to shut down for overhaul in July 2022.

Many researchers have studied the working state of copper staves through methods such as production data analysis and establishing heat transfer calculation models [8–32]. Ito and his co-authors [12–14] established a two-dimensional visualization model to study the temperature of copper staves based on spatial distribution and temporal variation data. Wu [15] used a combination of heat transfer numerical simulation and artificial neural networks to establish an intelligent simulation model for blast furnace staves, and this model could be used for online monitoring of the working status of blast furnace cooling staves. Lu [16] conducted heat transfer analysis and numerical simulation on the copper staves of the bosh and waist of the No. 2 blast furnace at Nangang and developed monitoring software with a slag thickness warning function. Liu [17] established a heat transfer model for a blast furnace stave, simulated the regeneration process of the slag crust on the hot surface of the stave using element birth and death technology in ANSYS, and analyzed the growth behavior of the slag crust after detachment. Jiao [18] constructed a hot-state experimental furnace for staves and studied the unsteady heat transfer process of blast furnace staves and the variation law of stave thermocouples under different conditions. Although the performance of the hot-surface slag crust varies with different smelting conditions, it is not possible to sample the hot-surface slag crust of blast furnace staves in actual operation. Many researchers use literature data such as slag thermal conductivity and hot-surface temperature to calculate important parameters required by their models, which results in inevitable errors and a lack of analysis of the appropriate slag crust thickness for blast furnaces.

This article focuses on the copper stave and its hot-surface slag crust in the bosh, waist, and lower shaft of a 3200 m³ blast furnace as the research object. The slag crust was sampled during a lowering of stockline operation and further was tested to obtain the thermal conductivity and soft melting temperature. Based on the above parameters, the slag crust thickness of the copper stave in the high-temperature zone of the blast furnace under different conditions is predicted by mathematical simulations. Consequently, a comparative analysis of the relationship between the thickness of slag crust on copper staves and the technical-economic indices of blast furnaces was conducted during the same time period. Finally, the appropriate thickness of hot-surface slag crust on copper staves in high-temperature areas was expected to be determined.

2. Sampling and Testing of Slag Crust from Copper Stave

The slag crust adhered to the hot surface of a copper stave has a very low thermal conductivity, which can provide good protection for copper staves in high-temperature areas. The thermal conductivity and reflowing temperature of the slag crust are the most important parameters for calculating the thickness of the slag adhesion layer. Currently, the thermal conductivity of the slag crust is generally believed to be the range of

1–5 W (m K)⁻¹ [17,24]. It is mainly influenced by the slag crust's chemical composition or phase composition. There are significant differences in the composition of slag crust based on different raw material conditions. Samples were taken from the hot surface of the copper cooler in the high-temperature zone of a blast furnace, taking advantage of the opportunity of maintenance of the blast furnace stockline. In order to accurately predict the thickness of the slag crust on the copper stave of the blast furnace, the chemical composition of the slag crust was analyzed, and physical-chemical properties such as thermal conductivity and melting performance were also tested. Figure 1 shows the adhesion state of slag on the surface of the copper stave in the high-temperature zone of the lower shaft of the blast furnace. Figure 2 shows the morphology of the slag crust.

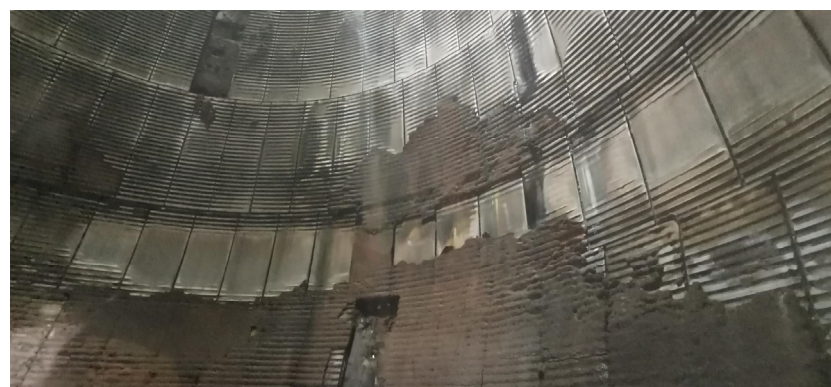


Figure 1. Slag crust adhered to the hot surface of the copper stave of the blast furnace.



Figure 2. Morphology of the slag crust sample.

2.1. Chemical Composition Analysis of Slag Crust

The slag crust samples on the hot surface of copper staves at different positions were tested, and the chemical compositions are shown in Table 1. The component analysis equipment was ICP-AES. It can be seen that in addition to a small amount of iron oxide, the main components in the slag crust are Al₂O₃, CaO, and SiO₂. These components easily form high-melting-point phases such as melilites and spinels, which are adhered to the hot surface of the copper stave and play a protective role on the cooling wall.

Table 1. Chemical composition of the slag crust sample (wt.%).

Sample No.	SiO ₂	Al ₂ O ₃	CaO	TFe	FeO	MgO	K ₂ O	Na ₂ O	TiO ₂	Zn	CuO	C
1	18.27	30.14	28.82	7.27	8.84	2.53	0.16	0.45	0.51	0.02	0.46	1.16
2	16.56	31.00	24.26	9.65	11.12	0.56	0.26	0.41	0.61	0.72	0.75	1.93
3	20.32	35.17	25.07	6.69	8.01	0.98	0.61	0.15	0.8	0.98	0.41	0.85
4	19.95	34.44	23.9	4.94	6.71	0.36	0.33	0.52	0.96	1.76	0.8	3.46

2.2. Thermal Conductivity of the Slag Crust

The procedure for determining the thermal conductivity of slag crust involved the following steps: (i) Grind both sides of the slag crust to provide a level surface in the thick-

ness direction, and thereafter place standard samples on a temperature-controlled plate. (ii) Enclose the outside side with thermal insulation cotton that possesses exceptionally low thermal conductivity to guarantee the full transfer of heat in the vertical direction of the sample throughout the test. (iii) Activate the temperature sensor to measure the temperature of the appropriate plate, as well as the temperatures of the upper and lower sides of the sample. (iv) Lastly, ascertain the thermal conductivity of the slag crust by employing the one-dimensional steady-state heat transfer method, based on the assumption of equal unidirectional heat flow intensity.

After the thermal conductivity of the slag crust samples was tested, the results (shown in Table 2) indicated that the actual thermal conductivity was between 1.45 and $1.55 \text{ W} (\text{m K})^{-1}$. As a result, the value of thermal conductivity of the slag crust was considered as $1.5 \text{ W} (\text{m K})^{-1}$ in this study.

Table 2. Thermal conductivity of the slag crust samples.

Sample No.	Thermal Conductivity $\text{W} (\text{m}\cdot\text{K})^{-1}$
1	1.451
2	1.526
3	1.541
4	1.495

2.3. Melting Performance of the Slag Crust

The melting test of a sample of the hot-surface slag crust was conducted as follows: The powdered slag crust sample (particle size $< 0.075 \text{ mm}$) was pressed into a cylindrical sample of $\varphi 6 \text{ mm} \times 6 \text{ mm}$ under a pressure of 10 MPa using a pressing machine. After that, the cylindrical sample was vertically placed on the support plate of the corundum boat in the experimental furnace. The high-temperature resistance furnace used molybdenum disilicide rods as heating materials. The corundum boat supporting the sample was kept in the isothermal zone of the corundum tube inside the furnace and then sealed with an insulation ring. The experimental samples were heated from room temperature to 1600°C , with a heating rate of $10^\circ\text{C}/\text{min}$ from room temperature to 1200°C and then $3^\circ\text{C}/\text{min}$ from 1200°C to 1600°C . High-purity N_2 was introduced as a protective gas with a gas flow rate of 0.8 L/min during the entire heating process. High-temperature photography was performed to record the melting process of the sample, as shown in Figure 3. The softening temperature (ST), hemispherical point temperature (MT), and flow point temperature (FT) of the slag crust samples were tested as shown in Table 3. According to Table 3, the average softening temperature, hemispherical point temperature, and flow point temperature of the slag crust samples were 1434.5°C , 1439.9°C , and 1468.1°C , respectively. Considering that a temperature below the softening temperature is necessary for the slag crust to adhere and not easily peel off, and the temperature error was $\pm 5^\circ\text{C}$, the hot-surface temperature of the slag crust was set to 1430°C during the mathematical simulation in the next step.

Table 3. Melting performance of the slag crust samples.

Sample No.	ST ($^\circ\text{C}$)	MT ($^\circ\text{C}$)	FT ($^\circ\text{C}$)
1	1434.1	1441.8	1466.9
2	1449.3	1454.3	1479.3
3	1432.2	1436.5	1464.2
4	1422.5	1427.1	1462.0

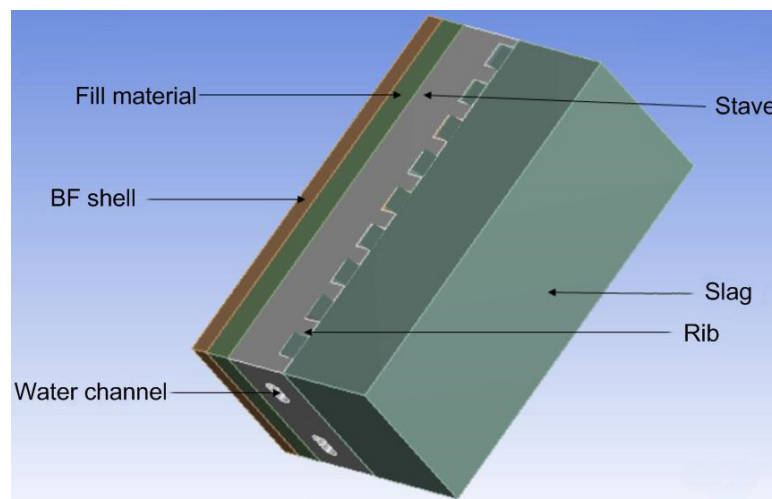


Figure 3. Geometry model of the heat transfer around copper stave.

3. Simulation of Thickness of the Slag Crust on Copper Stave

3.1. Model Assumptions

Taking the copper stave in the high-temperature area into account, a mathematical model for heat transfer of the copper stave was appropriately simplified and established. During the production process of a blast furnace, over 98% of the heat transferred from the slag crust to the copper cooling wall is carried away by cooling water [24]. The model assumes the following: (1) a certain thickness of refractory ramming material is filled between the furnace shell and the stave body, ignoring small structures such as fixed bolts and cooling water pipes outside the wall; (2) the blast furnace is in the middle and late campaigns, the hot-surface brick lining on the stave has completely disappeared, and the thickness of the slag is taken to exclude the thickness of the rib; (3) the heat conduction processes between the furnace shell and the filling material, between the filling material and the stave, and between the stave and the slag crust is ideal, ignoring the contact thermal resistance; (4) the width of the wall is relatively negligible small compared to the diameter of the furnace shell curvature, so the influence of the curvature of the furnace shell and wall is ignored, and a Cartesian coordinate system is used for modeling; (5) the furnace shell is in contact with air at the same temperature, and the cooling water flowing through the surface of the channel is uniform; (6) the thickness of the slag crust on the hot surface of the stave is consistent and in a steady state; (7) the heat transfer coefficients between the outer surface of the furnace shell and the air, as well as the heat transfer coefficients between the cooling water and the inner wall of the water channel, are constant.

3.2. Boundary Conditions and Parameters

The temperature of the hot-surface slag crust is set at 1430 °C. The air temperature is set at 30 °C, and the heat is mainly carried away by cooling water. The proportion of heat transferred into the air through the furnace shell is very small, so the comprehensive heat transfer coefficient of air is adopted as $11.0 \text{ W} (\text{m}^2 \cdot ^\circ\text{C})^{-1}$ [17]. The convective heat transfer coefficient between the cooling water and the stave needs to be determined by the structure of the cooling water channel and the physical properties of the water. The water velocity v is 1.7 m/s, and the equivalent diameter d of the cooling water channel inside the stave is 0.058 m. For example, when the cooling water temperature is 40 °C, the kinematic viscosity coefficient of the cooling water η is $0.659 \times 10^{-6} \text{ m}^2/\text{s}$, the thermal conductivity of cooling water λ is $0.633 \text{ W} (\text{m} \cdot \text{K})^{-1}$, and the Prandtl (Pr) number is 4.34. Re is the Reynolds number. The corresponding Reynolds number is

$$Re = \frac{vd}{\eta} = 1.496 \times 10^5 > 10^4 \quad (1)$$

The cooling water channel is subjected to forced convection inside the pipe, while the cooling water is turbulent. The following formula is used for calculation [25]:

$$Nu = 0.023Re^{0.8}Pr^{0.4} = \frac{hd}{\lambda} \quad (2)$$

where Nu is Nusselt number.

The convective heat transfer coefficient h is calculated as $6230 \text{ W} (\text{m}^2 \cdot ^\circ\text{C})^{-1}$.

3.3. Simulation and Validation of the Slag Crust Thickness

The geometry model of heat transfer around copper stave is shown in Figure 3. In the model, thermal conductivity is the only form of heat transfer, and the mathematical expression describing the temperature field in a solid body is the thermal conductivity differential equation. In a Cartesian coordinate system, when the thermal conductivity of an object is constant, the form of the thermal conductivity differential equation is

$$\frac{\partial t}{\partial \tau} = a \left(\frac{\partial^2 t}{\partial x^2} + \frac{\partial^2 t}{\partial y^2} + \frac{\partial^2 t}{\partial z^2} \right) + \frac{q_v}{\rho C_p} \quad (3)$$

where t is temperature, $^\circ\text{C}$; τ is time, s ; a is the thermal diffusion coefficient, m^2/s ; q_v is the intensity of the internal heat source, W/m^3 ; ρ is density, kg/m^3 ; C_p is specific heat capacity, $\text{J}(\text{kg} \cdot ^\circ\text{C})^{-1}$.

The thermal conductivity differential equation can be expressed as follows without an internal heat source and under steady-state conditions:

$$\frac{\partial^2 t}{\partial x^2} + \frac{\partial^2 t}{\partial y^2} + \frac{\partial^2 t}{\partial z^2} = 0 \quad (4)$$

The finite difference method is used to solve the steady-state three-dimensional heat conduction problem, assuming other data parameters remain unchanged. Then, the temperature distribution of the stave can be calculated for slag crust thickness by using computer programming with the Gauss–Seidel iteration method. The finite difference method replaces derivatives with difference quotients in differential equations, transforming them into corresponding difference equations and obtaining approximate solutions of the differential equations. To solve thermal conductivity problems using the finite difference method, the solution area must first be divided into a finite number of small grid elements. Usually, the intersection of grid lines is called a node, and the distance between nodes is measured in steps. Here, a cubic cell of $1 \text{ mm} \times 1 \text{ mm} \times 1 \text{ mm}$ is adopted for the grid division. In Equation (5), $t(i, j, k)$ is the temperature of node (i, j, k) . The temperature calculation equation for the internal nodes (i, j, k) is

$$t_{i,j,k} = \frac{1}{6} (t_{i+1,j,k} + t_{i-1,j,k} + t_{i,j+1,k} + t_{i,j-1,k} + t_{i,j,k+1} + t_{i,j,k-1}) \quad (5)$$

By setting the initial values of different internal nodes for verification, the tolerance in the last two neighbor iterations is controlled within $0.00001 \text{ }^\circ\text{C}$ at the end of the iteration. The difference between the initial node temperature calculations at $1430 \text{ }^\circ\text{C}$ and $42 \text{ }^\circ\text{C}$ is within $0.1 \text{ }^\circ\text{C}$, ensuring that the calculation accuracy meets the requirements.

During normal manufacture of the blast furnace, the flow rate and temperature of the cooling water are usually constant. The temperatures of different measurement sites of the stave vary with the different thicknesses of the slag crust. The flow rate of the cooling water of the blast furnace in this article is 1.7 m/s , and the temperature of the cooling water is around $42 \text{ }^\circ\text{C}$. The relationship between the temperature measurement site of the stave and the thickness of the slag crust is shown in Figure 4.

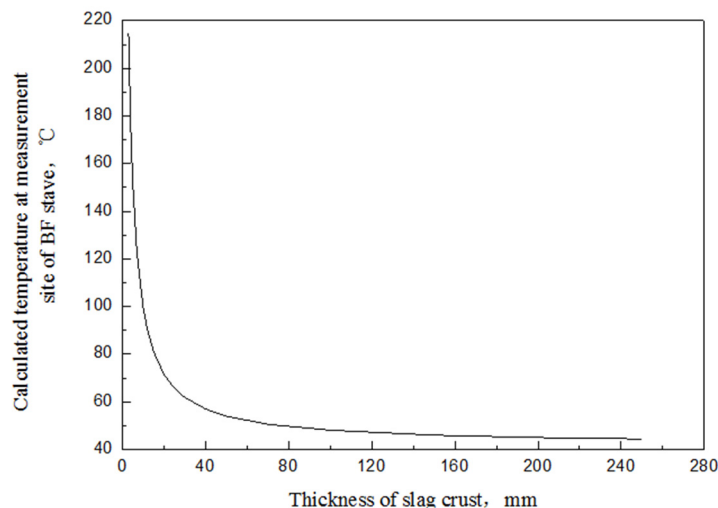


Figure 4. The temperature of the measurement site of the stave in dependence on the thickness of slag crust.

The actual temperatures at different measurement sites of the copper stave were measured before the shutdown and maintenance of the blast furnace, and the slag crust thickness was measured and validated after the dropping of the stockline. The cooling water reached 55 °C, and the flow rate was normal since some of the equipment in the blast furnace's cooling water heat exchanger needed maintenance when the stockline was being dropped. Using the above model, the thickness of the slag crust at the sampling location was calculated based on the temperature measurement of the copper stave. As shown in Figure 5, the results of the prediction model are accurate and can meet blast furnace requirements, as evidenced by the good agreement between the calculation results and the actual measurement findings. The temperatures of the copper stave in the high-temperature zone of the blast furnace were between 91 and 126 °C at the temperature measurement sites. During the stockline dropping, the slag crust of the stave was extremely thin, and its temperature was high. The thicknesses of 18 slag crust samples range from 8.8 to 22.8 mm, and the corresponding simulated slag crust thicknesses range from 9.1 to 17.4 mm, with minor inaccuracies. The comparison of actual and predicted slag crust thicknesses at the four measurement sites is shown in Figure 5.

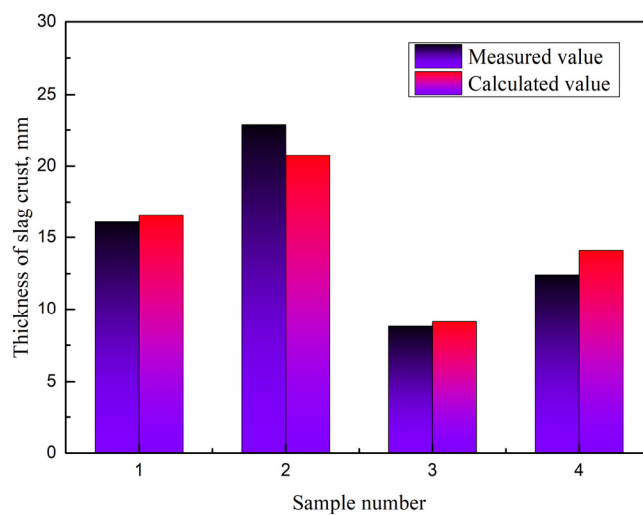


Figure 5. Comparison between measured and calculated thicknesses of slag crust samples.

4. Appropriate Thickness of the Slag Crust on Blast Furnace Stave

The bosh stave is the sixth cooling wall of this study's blast furnace, the waist cooling wall is the seventh part, and the lower staves of the furnace body are the eighth and ninth sections. With 48 cooling walls, 196 cooling water pipes, and 12 evenly spaced temperature monitoring sites per section, these four sections are copper staves in high-temperature regions.

4.1. Relationship between Slag Crust Thickness and Blast Furnace Indices

The slag crust thickness prediction model presented in this article was used to compute the mean thickness of the copper stave slag crust in the high-temperature region of the blast furnace. Then, the correlation computation was considered to analyze the technical and economic indicators of blast furnace production spanning from 2020 to the first half of 2022. The calculations are supposed to utilize data samples consisting of the daily average thickness of the slag crust, the number of material batches, the average blast volume, the average output, the average gas utilization rate, and the coke ratio. However, data acquired during the blast furnace shutdown should be removed from these calculations. Finally, the linear correlation coefficient between the thickness of the slag crust and these parameters was determined using the following formula:

$$r(X, Y) = \frac{Cov(X, Y)}{\sqrt{Var[X]Var[Y]}} \quad (6)$$

where $Cov(X, Y)$ is the covariance of X and Y , $Var[X]$ is the variance of X , and $Var[Y]$ is the variance of Y .

The results of the calculations indicate that the thickness of the slag crust has a strong correlation with the number of material batches, blast volume, production rate, and gas utilization rate. It is positively correlated with the coke ratio and negatively correlated with the other variables. Table 4 illustrates how significant technical and economic indices like blast furnace output and coke ratio would suffer as slag crust thickness rises.

Table 4. Correlation of slag crust thickness with blast furnace indices.

Parameter	Batches	Output Rate	Coke Ratio	Gas Utilization	Blast Volume
Correlation coefficient	-0.81	-0.78	0.66	-0.45	-0.78

The aforementioned phenomenon can be explained by the fact that a thicker slag crust results in a lower effective volume of smelting in the lower part of the blast furnace. This is detrimental to the smooth flow of furnace material and reduces the number of blast furnace material batches, blast volume, and output rate. In addition, anomalous furnace conditions are likely to arise, including irregular circumferential airflow, variations in the temperature field, and bonding in specific regions. As seen in Figure 6, limited blast volume causes insufficient airflow in the bosh section between the #3 and #4 iron notches (tapholes), which lowers the temperature and causes the bonding of a noticeably thicker slag crust in this area. These outcomes are detrimental to the development of indirect reduction in the blast furnace and lead to a lower gas utilization rate and higher coke ratio.

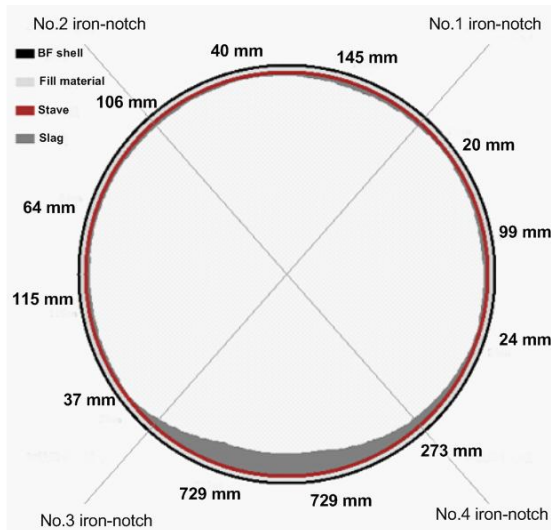


Figure 6. The calculated agglomeration of slag crust on the stave of the blast furnace bosh.

There will be an overall thickening of the slag crust in the blast furnace when there are several bonding locations. According to the computation results and analysis of blast furnace operation experience, the entire slag crust thickening in that section of the copper stave will occur when the slag crust thickness exceeds 250 mm in two-thirds of that section in the high-temperature area of the blast furnace. This will result in evident abnormalities in the blast furnace's operating parameters and indices. At this point, traditional adjustment techniques will be hard to manage and frequently call for blowdown treatment, causing significant losses in fuel, productivity, and financial gains.

4.2. Dependence of Slag Crust Thickness on the Stave Cooling Water Pipe Damage

Table 5 displays the average slag crust thickness and the number of damaged cooling water pipes in each section of the copper stave of the blast furnace based on statistics from 2020 to the first half of 2022. It is discovered that the cooling water pipes are more damaged the thinner the slag crust is, suggesting that the slag crust significantly protects the cooling wall. The sixth through eighth portions have few cooling water pipes, while the ninth section has a noticeably thin slag crust. The blast furnace's lengthy campaign is hampered by the serious damage to the cooling water pipes. Furthermore, damage to the cooling water pipes may result in water leaks inside the blast furnace, necessitating a break from the operation of the furnace in order to repair the pipes. This is not good for the blast furnace's long-term stability or efficient operation. Therefore, 150–200 mm is recommended as the suitable average thickness of slag crust, taking into account the technical indices of blast furnace output and the lengthy campaign of the blast furnace.

Table 5. The number of damaged cooling water pipes and the corresponding slag crust thickness.

Location	6th Section	7th Section	8th Section	9th Section
Thickness of slag crust (mm)	179.3	150.2	173.0	113.6
Number of damaged cooling water pipes	10	25	21	75

5. Conclusions

1. Slag crust samples were extracted from the hot surface of the copper stave in the high-temperature area, taking advantage of the blast furnace stockline's maintenance opportunity. The slag crust's chemical composition, thermal conductivity, and melting capability were examined. The slag crust has a thermal conductivity of

- 1.45–1.55 W (m K)⁻¹. Its flow temperature (FT), hemispherical temperature (MT), and softening temperature (ST) are 1468.1 °C, 1434.5 °C, and 1439.9 °C, respectively.
2. A mathematical model for the heat transfer of the copper stave was constructed using the copper stave in the high-temperature area of the blast furnace as the research object. The model was confirmed using real data gathered from the dropping of the stockline, and the temperature measurement points of the stave corresponding to various slag crust thicknesses during typical blast furnace production were computed. The outcomes of the computation and the measurement agreed fairly well.
 3. By examining the blast furnace output data from 2020 to 2022 and calculating the average thickness of the slag crust, it was discovered that the better the indices, the smaller the slag, but the greater the chance of cooling water pipe damage. The appropriate average slag thickness should be between 150 and 200 mm, taking into consideration both the long campaign and the technical indices of the blast furnace.

Author Contributions: Conceptualization, W.Z. and Z.X.; methodology, D.L.; validation, D.L. and C.S.; formal analysis, D.L.; writing—original draft preparation, D.L. and W.Z.; writing—review and editing, D.L., W.Z., and Z.X.; supervision, Z.X. and L.C.; project administration, D.L. and L.C. All authors have read and agreed to the published version of the manuscript.

Funding: The authors gratefully acknowledge the financial support from Hubei Provincial Key Technologies R & D Program (2022BCA058) as well as the Natural Science Foundation from Hubei Province (No. 2022CFB628).

Data Availability Statement: The data presented in this study are available on request from the corresponding author. The data are not publicly available due to privacy policy of Baowu Group.

Conflicts of Interest: Authors Dongliang Liu and Lingkun Chen were employed by the company Baosteel Central Research Institute (R&D Center of Wuhan Iron & Steel Co., Ltd.), Author Chunhui Song was employed by the company Wuhan Branch of Xiangyang Heavy Equipment Materials Co., Ltd. The remaining authors declare that the research was conducted in the absence of any commercial or financial relationships that could be construed as a potential conflict of interest.

References

1. Zhang, W.; Dai, J.; Li, C.Z.; Yu, X.B.; Xue, Z.L.; Saxén, H. A review on explorations of the oxygen blast furnace process. *Steel Res. Int.* **2021**, *92*, 2000326. [[CrossRef](#)]
2. Li, J.Q.; Li, C.Z.; Zhang, W.; Zhang, J.H.; Xue, Z.L. Material, energy and exergy flows of the oxygen blast furnace process with sintering flue gas injection. *J. Clean. Prod.* **2022**, *371*, 133294. [[CrossRef](#)]
3. Zhang, H.; Jiao, K.X.; Zhang, J.L.; Chen, Y.B. A new method for evaluating cooling capacity of blast furnace cooling stave. *Ironmak. Steelmak.* **2019**, *46*, 671–681. [[CrossRef](#)]
4. Deng, Y.; Liu, R.; Zhang, J.L.; Jiao, K.X. Manufacturing technology and application of cooling stave in blast furnace. *Metall. Res. Technol.* **2020**, *117*, 504. [[CrossRef](#)]
5. Fan, X.Y.; Jiao, K.X.; Zhang, J.L.; Wu, S.R.; E, D.Y.; Yan, B.G. Characterization and Properties of Scaffold in a Dissected Blast Furnace Hearth. *ISIJ Int.* **2019**, *59*, 2205–2211.
6. Zhang, W.; Li, K.; Dong, J.H.; Li, C.Z.; Liu, A.H.; Zhang, J.H.; Xue, Z.L. Kinetic triplet from low-temperature carburization and carbon deposition reactions. *J. Iron Steel Res. Int.* **2022**, *29*, 1545–1558. [[CrossRef](#)]
7. Li, F.G.; Zhang, J.L. Research on the Influence of Furnace Structure on Copper Cooling Stave Life. *High Temp. Mater.* **2019**, *38*, 1–7. [[CrossRef](#)]
8. Ni, A.; Li, C.Z.; Zhang, W.; Xiao, Z.X.; Liu, D.L.; Xue, Z.L. Investigation of the hearth erosion of WISCO No. 1 blast furnace based on the numerical analysis of iron flow and heat transfer in the hearth. *Metals* **2022**, *12*, 843. [[CrossRef](#)]
9. Zuo, H.B.; Wang, Y.J.; Wang, X.B. Damage Mechanism of Copper Staves in a 3200 m³ Blast Furnace. *Metals* **2018**, *8*, 943. [[CrossRef](#)]
10. Wu, T.; Cheng, S. Model of Forming-Accretion on Blast Furnace Copper Stave and Industrial Application. *J. Iron Steel Res. Int.* **2012**, *19*, 1–5. [[CrossRef](#)]
11. Xiang, Z.Y.; Wang, X.L. *Blast Furnace Design—Theory and Practice of Ironmaking Process Design*; Metallurgical Industry Press: Beijing, China, 2014; p. 388.
12. Masahiro, I.; Shinroku, M.; Kazumoto, K.; Makoto, I. *Development of Visual Evaluation and Numerical Analysis System of Blast Furnace*; Nippon Steel Technical Report No. 89; Nippon Steel: Tokyo, Japan, 2004; pp. 38–45.
13. Shinroku, M.; Masahiro, I.; Masaaki, N.; Kazumoto, K.; Makoto, I.; Nozomi, S.; Kenko, U.; Harutoshi, O. *Development of the Visualizing Information Technique of Blast Furnace Operation*; Nippon Steel Technical Report No. 96; Nippon Steel: Tokyo, Japan, 2006; pp. 96–102.

14. Shinroku, M.; Masahiro, I.; Atsushi, I. *Development of Visualizing System of Blast Furnace Operation and Application to Operation*; Nippon Steel Technical Report; Nippon Steel: Tokyo, Japan, 2015; pp. 245–253.
15. Wu, L.J.; Xu, X.; Zhou, W.G. Study on Intelligent Monitoring Methodology for Blast Furnace Stave. *Iron Steel* **2008**, *43*, 13–16.
16. Lu, Z.A.; Wu, L.J.; Zhou, W.G.; Sun, G.P.; Xiong, L.Y. Intelligent Monitoring of Blast Furnace Stave Hot Surface Status. *Iron Steel* **2010**, *45*, 22–26.
17. Liu, Z.X.; Li, Z.; Chai, Q.F.; Lü, Q. Heat Transfer Analysis of Slag Skull Growth for BF Copper Stave. *Iron Steel* **2010**, *45*, 12–15.
18. Jiao, K.X.; Zhang, J.L.; Zuo, H.B.; Shen, M.; Tie, J.Y.; Li, F.G. Thermal Trial Analysis on Unsteady Heat Transfer for Blast Furnace Cooling Stave. *Iron Steel* **2014**, *49*, 32.
19. Maarten, G.; Rénard, C.; Ivan, K.; Oscar, L.; John, R. *Modern Blast Furnace Ironmaking*; IOS Press: Delft, The Netherlands, 2015; pp. 172–174.
20. Yasuo, O.; Yaasuhito, S.; Junichiro, V.; Masakazu, N.; Tsutomu, F. *Blast Furnace Phenomena and Modelling*; Elsevier Applied Science Publishers Ltd.: Amsterdam, The Netherlands, 1987; pp. 207–220.
21. Andrew, S.; Afashin, S.; Ian, C.; Maciej, J.; Rick, B.; Barry, H. Preserving Copper Staves and Extending Blast Furnace Campaign Life. In Proceedings of the AISTech 2014 Proceedings, Indianapolis, IN, USA, 5–8 May 2014; pp. 715–719.
22. Cegna, G.; Lingiardi, O.; Musante, R. Copper Stave Wear-Ternium Siderar BF2 Experience. In Proceedings of the AISTech 2014 Proceedings, Indianapolis, IN, USA, 5–8 May 2014; pp. 683–687.
23. Afshin, S.; Barry, H.; Brad, D.; Koorosh, M. Accurate and Flexible NDT Measurements of Copper and Cast Iron Stave Thickness in the Blast Furnace. In Proceedings of the AISTech 2013 Proceedings, Pittsburgh, PA, USA, 6–9 May 2013; pp. 629–636.
24. Che, Y.; Sun, P.; Li, L.P.; Sun, B.; Guo, T.Y. The development and application of the inner profile management model in Angang's BF lined with the Copper stave. *Ironmaking* **2007**, *26*, 18–21, 32.
25. Zhang, X.Z. *Metallurgical Transmission Principles*; Metallurgical Industry Press: Beijing, China, 1998; pp. 295–300, 432.
26. Liu, D.L.; Chen, L.K. Development and application of No. 7 BF condition diagnosis system in WISCO. *Metall. Ind. Autom.* **2021**, *45*, 26–33.
27. Xu, X.; Wu, L.J.; Yuan, Z.K. Thermal test and numerical simulation of cooling stave with internal ribbed tube. *J. Iron Steel Res.* **2022**, *29*, 1197–1204. [[CrossRef](#)]
28. Liu, S.H.; Hua, J.M. Analysis on the operation and maintenance practice of Baosteel's BF copper cooling stave. *Ironmaking* **2020**, *39*, 1–6.
29. Shao, Q.; Lin, S.; Zhang, F. Practice of furnace type management for Benxi Steel's No. 6 blast furnace. *Ironmaking* **2021**, *40*, 44–48.
30. Zeng, W.T.; Zhang, Q.X. Maintenance technology for operating profile of BF with copper stave. *Ironmaking* **2021**, *40*, 6–10.
31. Du, P.; Lei, M.; Jiang, D.W.; Wang, Z.Y.; Zhang, J.L.; Xu, Z. Clustering analysis of blast furnace profile based on blast furnace cooling stave temperature. *Metall. Ind. Autom.* **2023**, *47*, 109–115.
32. Shen, D.; Chen, M.J.; She, J.P. Discussion on optimization of BF copper cooling stave design. *Ironmaking* **2020**, *39*, 7–12.

Disclaimer/Publisher's Note: The statements, opinions and data contained in all publications are solely those of the individual author(s) and contributor(s) and not of MDPI and/or the editor(s). MDPI and/or the editor(s) disclaim responsibility for any injury to people or property resulting from any ideas, methods, instructions or products referred to in the content.